Available online at www.sciencedirect.com
SCIENCE DIRECT®
Earth and Planetary Science Letters 243 (2006) 476–488
EPSL
www.elsevier.com/locate/epsl

High resolution evidence for linkages between NW European ice sheet instability and Atlantic Meridional Overturning Circulation

V.L. Peck [a,*], I.R. Hall [a,*], R. Zahn [b,*,1], H. Elderfield [c], F. Grousset [d], S.R. Hemming [e], J.D. Scourse [f]

[a] *School of Earth, Ocean and Planetary Science, Main Building, Park Place, Cardiff University, Cardiff CF10 3YE, UK*
[b] *Institució Catalana de Recerca i Estudis Avançats (ICREA), and Universitat Autonoma de Barcelona, 08193, Bellaterra, Spain*
[c] *Department of Earth Sciences, Cambridge University, Downing Street, Cambridge CB2 3EQ, UK*
[d] *Departement de Geologie et Oceanographie, Université Bordeaux I, Avenue des Facultés, 33405 Talence cedex, France*
[e] *Department of Earth and Environmental Sciences, Lamont–Doherty Earth Observatory, 61 Route 9W Palisades, NY 10964, USA*
[f] *School of Ocean Sciences, University of Wales (Bangor), Menai Bridge, Angelsey, LL59 5AB, UK*

Received 12 June 2005; received in revised form 19 December 2005; accepted 20 December 2005
Available online 3 February 2006
Editor: E. Boyle

Abstract

Published studies show that ice rafted debris (IRD) deposition preceding Heinrich (H) events H1 and H2 in the NE Atlantic was derived from the NW European ice sheets (NWEIS), possibly offering clues about ice sheet sensitivity and stability, and the mechanisms that caused periodic collapse of the Laurentide Ice Sheet (LIS). We present detailed lithological and geochemical records, including radiogenic isotope fingerprinting, of IRD deposits from core MD01-2461, proximal to the last glacial British Ice Sheet (BIS), demonstrating persistent instability of the BIS, with significant destabilisation occurring 1.5–1.9 kyr prior to both H1 and H2, dated at 16.9 and 24.1 kyr BP, respectively, in the NE Atlantic. Paired Mg/Ca and $\delta^{18}O$ data from the surface dwelling *Globigerina bulloides* and subsurface dwelling *Neogloboquadrina pachyderma* sinistral are used to determine late-glacial variability of temperature, salinity and stratification of the upper water column. A picture emerges that the BIS was in a continuing state of readjustment and never fully reached steady state. Increased sea surface temperatures appear to have triggered the episode of NWEIS instability preceding H1. It seems most probable that the so-called 'precursor' events were not linked to the H events. However, if response to a common thermal forcing is considered, an increased response time of the LIS, up to ~2 kyr longer than the NWEIS, may be inferred. Negative salinity excursions of up to 2.6 indicate significant incursions of melt water associated with peaks in NWEIS instability. Decreased surface density led to a more stable stratification of the upper water column and is associated with reduced ventilation of intermediate waters, recorded in depleted epibenthic $\delta^{13}C$ (*Cibicidoides wuellerstorfi*). We suggest that instability and meltwater forcing of the NWEIS temporarily weakened Atlantic Meridional Overturning Circulation, allowing transient advance of southern-sourced waters to this site, prior to H events 1 and 2.

Keywords: NW European Ice Sheet; ocean–climate linkage; Atlantic Meridional Overturning Circulation; ice rafted debris; Heinrich events; ice sheet instability

* Corresponding authors.
E-mail addresses: peckvl@cf.ac.uk (V.L. Peck), hall@cf.ac.uk (I.R. Hall), rainer.zahn@uab.es (R. Zahn).
[1] Also at [a].

0012-821X/$ - see front matter © 2006 Elsevier B.V. All rights reserved.
doi:10.1016/j.epsl.2005.12.023

1. Introduction

Numerical modelling suggests that increases in freshwater flux of just 0.01 Sv, if routed to the centres of active deep-water convection, have the capability to cause considerable reduction in the Atlantic Meridional Overturning Circulation (AMOC), accounting for mean annual temperature changes of between 5–10 °C in the circum-North Atlantic region over a matter of decades [1]. The last glacial NW European ice sheets (NWEIS; comprising the British, Icelandic and Fennoscandian ice sheets) likely achieved a maximum ice volume of $\sim 10 \times 10^6$ km^3, approximately one third that of the North American, Laurentide ice sheet (LIS) [2], often considered to be the principal driver behind millennial scale variability in AMOC during the last glacial period [3–5]. Rather than the volume of these freshwater reservoirs however, it is the location of the NWEIS close to the main North Atlantic convection centres, that enhances their potential to perturb AMOC and climate during episodes of accelerated ice sheet melting.

Despite intensive research into Heinrich (H) events (see recent review [6]) and Dansgaard–Oeschger (D–O) climatic oscillations that are associated with ~1.5 kyr ice rafted detritus (IRD) cycles in the NE Atlantic (e.g. [7,8]), there is no clear consensus on the underlying mechanism that caused these periodic phenomena. Hypotheses relating to H event initiation include external forcing, probably intimately linked to perturbations of AMOC dynamics (e.g. [9]), and the internal dynamics of the LIS [10,11]. Modelling [10,11] and lack of significant D–O frequency surging of the Hudson Strait ice stream [12] suggest that the LIS was relatively stable and largely immune to high-frequency (climate) forcing, favouring internal instabilities as the trigger for periodic LIS collapse every 7–10 kyr [10,13]. Conversely, the sensitivity of the smaller NWEIS of the last glacial is well documented [14–16]. Recent studies have identified NWEIS instability prior to H events 1 and 2 [17–19], possibly supporting a common external triggering mechanism of H events, assuming individual ice sheet response times were, in part, proportional to ice sheet size/extent of marine margin. Understanding the forcing and climatic feedbacks that propel these millennial scale cycles, including their interference with AMOC, is crucial for the development of predictive climate models [1].

Here we present evidence from a marine sediment core for NWEIS variability preceding H1 and H2 (~16.8 and ~24.0 kyr BP; [20,21]). Multi-proxy foraminiferal and lithologic geochemical analyses allow us to document the variability of the British (BIS), East Greenland/Icelandic (EGIIS) and Laurentide ice sheets in fine detail in a framework of AMOC variability.

2. Materials and methods

Sediment core MD01-2461 was recovered from the north-western flank of the Porcupine Seabight (51° 45′ N, 12° 55′W) in a water depth of 1153 m (Fig. 1). The site is ideally located to monitor BIS variability as it is close to the last glacial Irish Sea ice stream, a principal outlet glacier draining the BIS [22]. As previous studies illustrate, a cyclonic surface gyre circulation in the subpolar North Atlantic routed iceberg drifts from the circum-North Atlantic ice sheets to this region [23–25] so that the core records also monitor IRD derived from other North Atlantic margins.

The chronology of MD01-2461 is based on 15 monospecific foraminifera (*Globigerina bulloides*, or *Neogloboquadrina pachyderma* sinistral) AMS ^{14}C dates. Radiocarbon ages were calibrated to calendar years before present (yr BP) using the CALIB programme (version 5.0.1 with the MARINE04 data set), incorporating a 400 yr correction for marine reservoir age [26] (Table 1). However, comparison of the relative abundance of *N. pachyderma* sin. (%; an apparent relative sea surface temperature (SST) proxy, [27]) with the GISPII δ^{18}O record [28] (Fig. 2b, c) suggests that the constant ^{14}C-reservoir assumption is likely incorrect. The climate-based correlation ($r^2 = 0.829$) suggests that the 400-yr ^{14}C-reservoir correction is a considerable

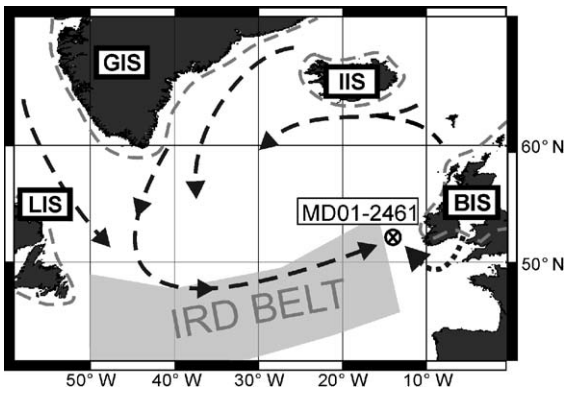

Fig. 1. Location of core MD01-2461 at the northeastern extent of the Ruddiman belt of preferential IRD accumulation [25]. Dashed black lines indicate likely routes of icebergs derived from circum-North Atlantic ice sheets due to an anti-clockwise surface gyre during the last glacial [23,25]. Dashed grey lines represent last glacial maximum ice sheet (IS) extent. B — British; I — Icelandic; G — Greenland; L — Laurentide. Dashed grey lines represent last glacial maximum ice sheet (IS) extent.

Table 1
Radiocarbon ages for MD02-2461

Laboratory code	Material	Depth (cm)	^{14}C age (yr BP)	Error age (±1σ yr)	Calendar age (a BP)
SUERC-3302	*N. pachyderma* sin.	196.5	11,032	39	12,709
SUERC-3303	*G. bulloides*	208.5	12,551	46	13,992
SUERC-3306	*N. pachyderma* sin.	228.5	11,950	43	13,337 [a]
SUERC-3287	*N. pachyderma* sin.	244.5	14,530	58	16,819
SUERC-3307	*N. pachyderma* sin.	276.5	15,118	64	17,692
SUERC-3308	*N. pachyderma* sin.	302.5	15,518	63	18,564
SUERC-3309	*N. pachyderma* sin.	324.5	15,174	60	17,586 [a]
SUERC-3288	*N. pachyderma* sin.	356.5	17,130	77	19,993
SUERC-3289	*G. bulloides*	392.5	18,233	87	21,053
SUERC-3290	*N. pachyderma* sin.	412.5	18,665	89	21,688
SUERC-3292	*N. pachyderma* sin.	436.5	19,128	94	22,287
SUERC-2278	*G. bulloides*	478.0	20,193	118	23,702
SUERC-2279	*N. pachyderma* sin.	528.5	20,931	129	24,577
SUERC-2275	*N. pachyderma* sin.	570.5	21,565	128	25,647
SUERC-2274	*N. pachyderma* sin.	602.5	22,234	147	25,792

[a] Age reversals removed.

underestimate, with offset between the tuned and ^{14}C-based age model increasing following H2 and the last glacial maximum (LGM; Fig. 2a). Elevated ^{14}C-marine reservoir ages have previously been interpreted from North Atlantic sediments, reflecting sea-ice or meltwater cover reducing air–sea gas exchange and isotope equilibration [29–32]. Our correlation between *N. pachyderma* sin. % and the Greenland ice core palaeoclimatic record suggests ^{14}C-marine reservoir ages of up to ~2 kyr occurred at our site during periods of substantial meltwater release and ocean stratification. An additional consideration may be release of aged CO_2 during ice sheet melt [33]. Here, we use the age model derived from tuning the *N. pachyderma* sin. % record to GISPII δ^{18}O profile which provides a robust stratigraphy that is

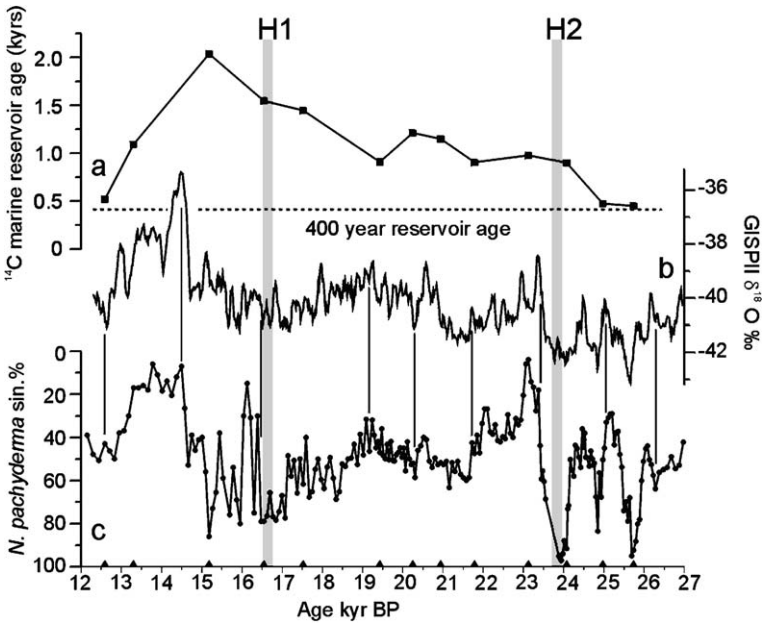

Fig. 2. Stratigraphic correlation between relative abundance of *N. pachyderma* sin. and GISPII ice core. (a) Suggested ^{14}C-marine reservoir ages determined from the age difference between calibrated ^{14}C ages and calendar years based on the correlation of *N. pachyderma* sin. % (c) with GISPII δ^{18}O [28] (b). Dashed line indicates the present day North Atlantic ^{14}C-marine reservoir age of 400 yr. Vertical lines indicate tie-points used for stratigraphic correlation. Black triangles in (c) indicate ^{14}C date. Grey bars locate H layers 1 and 2.

comparable with the Greenland ice core record and palaeoceanographic profiles from other North Atlantic core sites [34]. Sedimentation rates range between 12 and 60 cm kyr^{-1} yielding, at a sampling interval of 1–2 cm, a mean time step along the records of 60±30 yr.

Lithic grains >150 μm embedded within the silty clay sediment are considered to be ice rafted [7,25]. Through visual, lithological classification we distinguish between non-provenance specific quartz and haematite-coated grains, an East Greenland/Icelandic (EGIIS) assemblage of volcanic debris (pumice, black glass and basalt), LIS-sourced dolomitic carbonate [35], and a BIS assemblage (shale, dark carbonates and black limestone) sourced in part from Carboniferous formations that outcrop across much of Ireland. Chalk clasts occasionally associated with this BIS assemblage support an Irish Sea ice stream source, with Coniacian–Santonian age coccoliths (pers. comm. J. Young, Natural History Museum) suggesting erosion of the Celtic Shelf by the Irish Sea ice stream [cf. [18]].

As additional provenance fingerprints we use radiogenic isotopes ($^{143}Nd/^{144}Nd$) and $^{40}Ar/^{39}Ar$ ages of individual hornblende grains. The $^{143}Nd/^{144}Nd$ of the non-carbonate, >150 μm fraction was determined for 16 samples in the intervals associated with H2 and H1. Chemically separated Nd was analysed on a Finnigan MAT 261 mass spectrometer at Toulouse University, normalised and reported as ε_{Nd} following Grousset et al. [36].

Hornblende grains were picked from the >150 μm size fraction wherever present. Grains were co-irradiated with hornblende monitor standard Mmhb (age=525 Myr; [37]) and $^{39}Ar/^{40}Ar$ ratios of individual hornblende grains were determined at the Ar geochronology laboratory at Lamont–Doherty Earth Observatory. Resulting ages have been corrected for mass discrimination, interfering nuclear reactions, procedural blanks and atmospheric Ar contamination [38–40]. The assignment of IRD assemblages to a specific ice sheet provenance is determined from the above suite of proxy-approaches and is discussed in detail elsewhere [41].

Upper water column temperature and vertical structure were determined through paired Mg/Ca and oxygen isotope analyses of surface dwelling *G. bulloides* and subsurface dwelling *N. pachyderma* sin. Samples of 50 specimens where available (not less than 20) were crushed, homogenised and split. Samples for Mg/Ca analysis were cleaned following Barker et al. [42] and analysed on an ICP-AES (Varian Vista) with a precision better than 0.4% (1σ; liquid standard), and sample reproducibility of ≤4%. Temperature calibration is discussed below (Section 3.2). All stable isotope analyses were made using a ThermoFinnigan MAT 252 with an external reproducibility of ≤0.08‰ for $\delta^{18}O$ and 0.03‰ for $\delta^{13}C$. Benthic isotope measurements were made on 1–4 specimens of *Cidicidoides wuellerstorfi* where possible.

3. Results and discussion

3.1. Ice sheet instabilities

An almost constant flux of IRD to the core site throughout the period 26.5–17 kyr BP suggests constant readjustment of the BIS marine margins. Within this time, four distinct episodes of ice sheet instability may be inferred from enhanced IRD flux (Fig. 3d). The H1 and H2 layers, centred at 24.1 kyr BP and 16.9 kyr BP, respectively, stand out in the records due to their high magnetic susceptibility (Fig. 3b; [23,43]) and the presence of distinctive dolomitic carbonate sourced from the Hudson Strait region of the LIS (Fig. 3g; [35]). Crustal debris derived from the Precambrian shield underlying the LIS is identified by ε_{Nd} values of <−24 (Fig. 3a) [17,44,45]. This is corroborated by the Palaeoproterozoic age range (1650–1900 Ma) of the Churchill Province which dominates the assemblages of hornblende grains extracted from each of these IRD layers in our core (Fig. 3c: H1, 84% n=13; H2, 82% n=29) [40]. These are the type H layers sensu strictu. At this site they are each only 1–6 cm thick and represent 100–300 yr within episodes of IRD deposition exceeding 2000 yr (H2) in the NE Atlantic. Given the apparent synchronicity of H layer deposition across the IRD belt (cf. H layer ages compiled in [6,34]) instability of the LIS and extensive iceberg discharge from the Hudson Strait lagged the regional increase in IRD deposition in the NE Atlantic by >1 kyr, consistent with the European 'precursor' events of Grousset et al. [17] and Scourse et al. [18]. The high resolution records, robust age model and multi-proxy investigation of ice–ocean interaction presented in this study allow more detailed interpretation and accurate dating of these 'precursor' events than previous studies have allowed.

Prior to H2, the first phase of ice sheet activity is marked by enhanced fluxes of EGIIS- and BIS-sourced IRD (Fig. 3e, f) at 26.2 kyr BP, with associated radiogenic ε_{Nd} of −5.6 (just above 'd', Fig. 3a) reflecting the strong volcanic contribution. This initial episode of NWEIS instability and IRD deposition occurred 1.9 kyr prior to the first appearance of Hudson Strait sourced debris at 24.25 kyr BP and lasted 400 yr. Enhanced deposition of BIS debris recommenced at 25.5 kyr BP and increased steadily for 300 yr with little

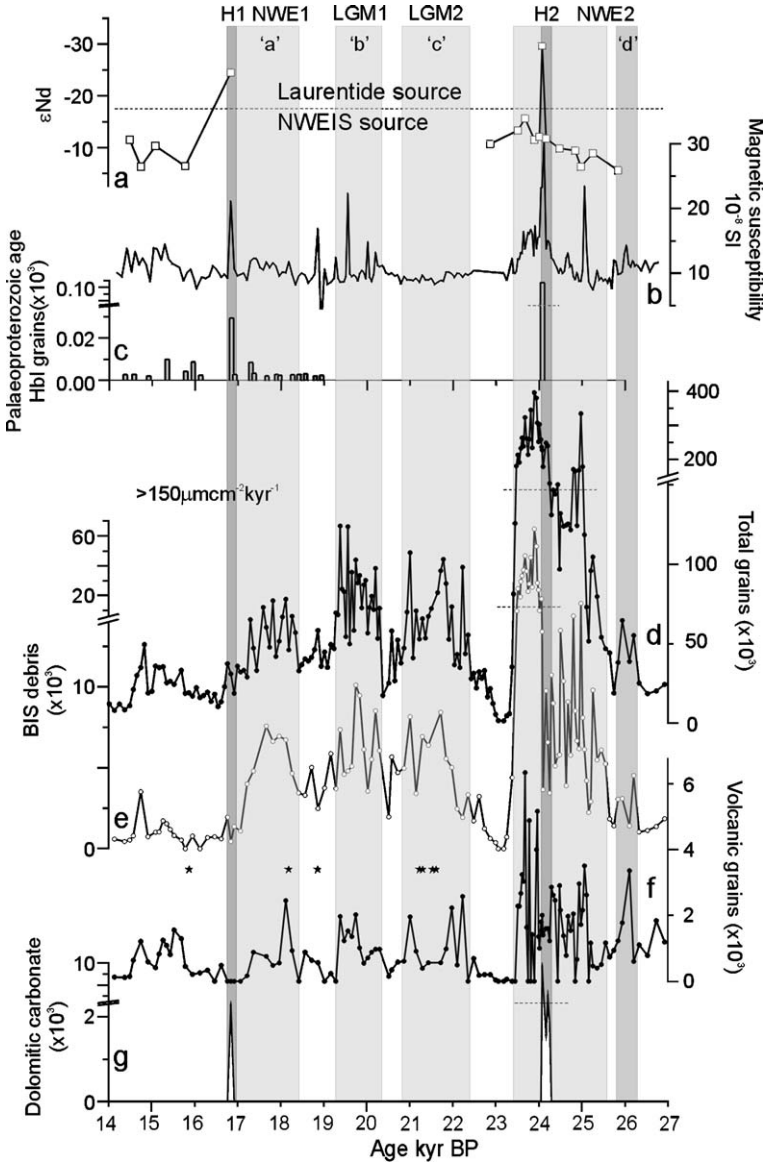

Fig. 3. Lithological and geochemical IRD records versus age from core MD01-2461. All measurements except magnetic susceptibility were made on the >150 μm fraction. All IRD counts are normalized to fluxes (grains g^{-1} × dry bulk density (g cm^{-3}) × sedimentation rate (cm kyr^{-1}) = grains cm^{-2} kyr^{-1}). (a) ε_{Nd} of silicate fraction, (b) whole-core magnetic susceptibility [43], flux of ice rafted (c) hornblende grains with Palaeoproterozoic (1650–1900 Ma) $^{40}Ar/^{39}Ar$ ages, (d) total grains, (e) BIS grains, (f) volcanic grains and (g) dolomitic carbonate grains to MD01-2461 (>150 μm cm^{-2} kyr^{-1}). Note break in axes. Stars in (e) denote depths where Upper Cretaceous Chalk is found. Vertical bars highlight dominance of IRD provenance; light grey = BIS is main IRD source; medium grey = significant contribution from EGIIS; dark grey = LIS signature is recorded. Acronyms are as follows: H, Heinrich Layer; NWE, NW European ice sheet sourced events (numbers refer to respective H layers). LGM, last glacial maximum. Letters a, b, c and d refer to correlative events of Bond and Lotti [7].

input from the EGIIS. IRD flux then rapidly increased, total IRD exceeding 350×10^3 grains cm^{-2} kyr^{-1} at 25.0 kyr BP. Increased fluxes of both volcanic and BIS debris, together with ε_{Nd} values of −6.3, suggest bimodal sourcing of IRD from both the BIS and EGIIS in this phase of considerable NWEIS instability lasting 300 yr. The timing of this peak in NWEIS instability recorded at MD01-2461 is, within the constraints of the age models, equivalent to that of the relatively radiogenic ε_{Nd} 'precursor' IRD peak at MD95-2002 in the Bay of Biscay [17], and the Celtic Shelf chalk-rich IRD peak at the Goban Spur [18]. Following this episode of substantial IRD deposition, the flux of volcanic debris decreased again while ε_{Nd}

values of −11 to −12, approaching the British Isles end member [45], became dominant for 900 yr, until the arrival of LIS-sourced icebergs and H layer deposition. This entire episode of NWEIS instabilities is termed NWE2 (Fig. 3).

Similar sequencing of NWEIS IRD deposition is observed prior to H1, NWE1. A significant influx of IRD derived from both the BIS and the EGIIS, commenced at 18.4 kyr BP, 1.5 kyr prior to the arrival of Hudson Strait debris. Dissimilar to NWE2, there is no substantial increase or peak in IRD flux, rather total IRD steadily decreases across NWE1, remaining low throughout the deposition of H layer 1 when total IRD was just 28×10^3 grains cm^{-2} kyr^{-1}, approximately a 10-fold reduction compared to H2 fluxes.

Two significant IRD layers of NWEIS derivation occurred between H1 and H2, commencing at ~22.4 kyr BP (LGM2) and ~20.3 kyr BP (LGM1). These intervals lasted 1.6 and 1.0 kyr, respectively. The peaks of these three most recent IRD events (LGM2, 1 and NWE1) present a periodicity of 1.5–1.6 kyr, likely correlating to peaks in volcanic and haematite-coated grains

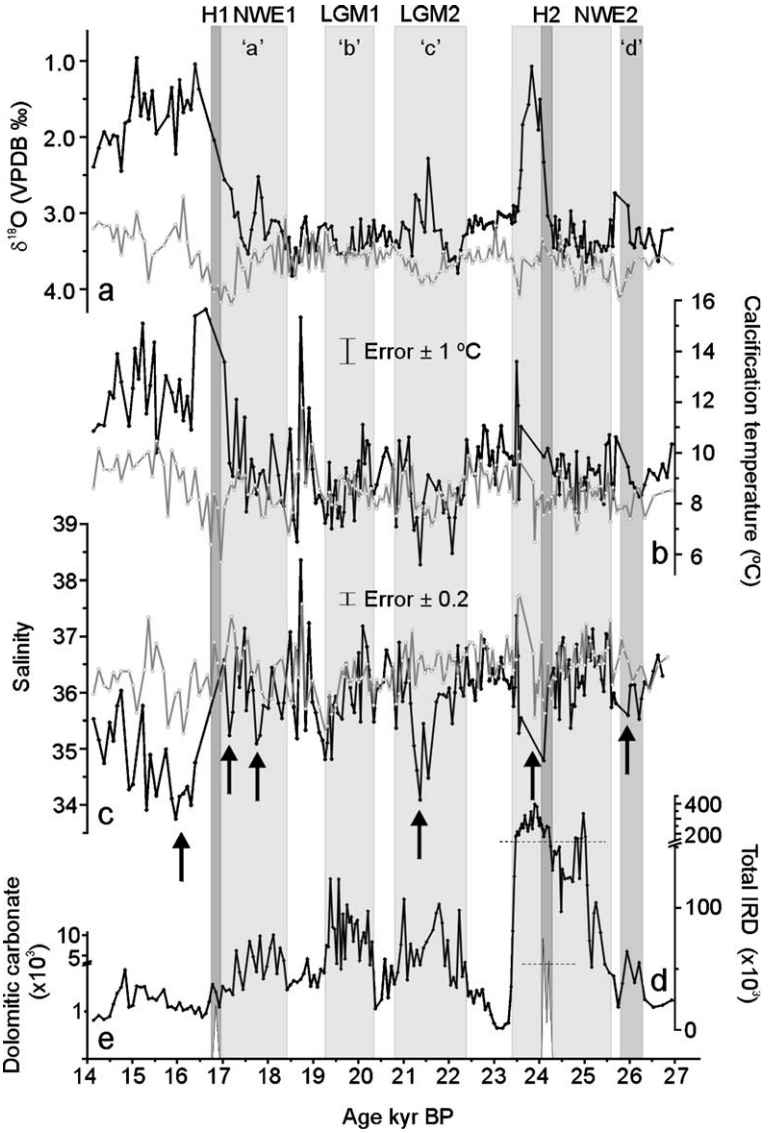

Fig. 4. Upper ocean climate records from core MD01-2461. (a) $\delta^{18}O$ of *G. bulloides* (black, closed circles) and *N. pachyderma* sin. (grey, open circles). (b) Calcification temperatures (°C) of *G. bulloides* (upper 60 m of water column; black, closed circles) and *N. pachyderma* sin. (100-200 m water depth; grey, open circles). (c) SSS (black, closed circles) and subsurface salinity (grey, open circles) based on *G. bulloides* and *N. pachyderma* sin., respectively. Flux of (d) total IRD, (e) dolomitic carbonate ($\times10^3$; per $cm^{-2}\,kyr^{-1}$) to MD01-2461. Vertical bars and abbreviations as Fig. 3. Meltwater pulses indicated with vertical arrows on (c).

recognised within the North Atlantic IRD belt ("a", "b" and "c" of [7]). IRD deposited at our core site from the first phase of NWE2, peaking at 25.9 kyr BP, may relate to "d" at ~23.0 ^{14}C kyr [7] and is labelled accordingly (Fig. 3), supporting synchronous instability of the NWEIS and potentially the south-eastern extent of the LIS also.

3.2. Surface, subsurface and intermediate water conditions associated with ice rafting events

Except for intervals where the δ^{18}O of *G. bulloides* and *N. pachyderma* sin. are identical around the LGM, *N. pachyderma* sin. consistently displays heavier δ^{18}O than *G. bulloides* (Fig. 4a), reflecting the greater depth and lower temperature habitat of *N. pachyderma* sin. As Hillaire-Marcel and Bilodeau [46] and Simstich et al. [47] we interpret similar δ^{18}O values of surface and subsurface species to represent intensive mixing of the upper water column. However, this interpretation requires that each species calcifies in equilibrium with seawater δ^{18}O and ambient temperature, or that possible disequilibrium calcification is known and corrected for. The carbonate–water temperature equation of Shackleton [48] is used to determine equilibrium calcite oxygen isotope composition from modern water column data (Fig. 5a; [49]). A factor of −0.27‰ is used to convert water on the SMOW scale to calcite on the VPDB (Fig. 5b). Assuming an average calcification depth of 30 m for *G. bulloides* [50], $\delta^{18}O_{G.\ bulloides}$ from core top specimens predict a summer (~July) growth season, within water temperatures averaging ~12 °C. This growth season is later than that of April–June predicted by Ganssen and Kroon [51], who assume *G. bulloides* isotopic temperatures reflect true SST, not the 0–60 m depth range within which the specimens calcified. Similar latitude core top $\delta^{18}O_{G.\ bulloides}$ from the Ganssen and Kroon data set (Fig. 5b; [51]) fit our core top values, reinforcing our interpretation of a summer bloom season at an average water depth of 30 m.

The lower limit of the present day summer thermocline, overlies the average depth of *N. pachyderma* sin. calcification, ~100–200 m [47,52–54], where there is negligible change in water temperature throughout the year (<0.6 °C). As fluxes in *N. pachyderma* sin. are tied to phytoplankton blooms [53], it is likely that the majority of *N. pachyderma* sin. calcified during a similar growth season to *G. bulloides* yet effectively record the mean annual temperature of subsurface waters [55]. Significant regional variability of vital effect, offsetting $\delta^{18}O_{N.\ pachyderma\ sin.}$ from equilibrium calcite, is determined from North Atlantic–Arctic Ocean core tops where *N. pachyderma* sin. currently thrive. Offsets range between 0‰ [56–58] and −1‰ [47,53,59,60]. The absence of *N. pachyderma* sin. from the top 1 m of MD01-2461 precludes attempts to determine possible $\delta^{18}O_{N.\ pachyderma\ sin.}$ disequilibria, yet it would appear that any offset at this site would certainly be <1‰, potentially zero [56]. From these considerations we assume that both planktonic species calcified in, or close to, isotopic equilibrium (cf. [46]).

Mg/Ca of foraminifers is proven to be an effective palaeotemperature proxy [61], but established calibrations for *G. bulloides* are not based on temperatures lower than ~10 °C. Applying the Mg/Ca–temperature calibration of Mashiotta et al. [62] to core top *G. bulloides* Mg/Ca, we derive summer SSTs 2 °C in excess of modern SST (13.7 °C [49]) and LGM SSTs of 10–11 °C, exceeding previous estimates for this region by up to 7 °C (e.g. [63]). These discrepancies suggest that the calibration of Mashiotta et al. [62] is unsuitable at our core site. As *N. pachyderma* sin. is absent in the core top it was not possible to assess the calibration of Nürnberg et al. [64] for this species.

To resolve these calibration issues we assume that the period 20–19 ka BP, when the δ^{18}O values of both *G. bulloides* and *N. pachyderma* sin. are broadly identical (Fig. 4a), represents an episode of upper water column mixing [46,47] in which both species were exposed to identical water mass and calcification temperatures. Using the exponential relationship between Mg/Ca and temperature, $Mg/Ca = A\exp(B \times T)$, and assuming a similar exponent value of 0.1 for both species [65], we determine a pre-exponent ratio *G. bulloides*:*N. pachyderma* sin. of 2.1. From modern SST (30 m) and core top Mg/Ca values we derive a pre-exponent of 0.68 for *G. bulloides* and, by virtue of the pre-exponent ratio of 2.1, 0.32 for *N. pachyderma* sin., assuming a fixed pre-exponent ratio across the glacial–interglacial transition. This calibration compares well with that of Barker and Elderfield [50] ($Mg/Ca = 0.72 \times e^{0.1T}$) for *G. bulloides* at 60°N in the North Atlantic. The *N. pachyderma* sin. Mg/Ca–temperature calibration effectively equates to the generic calibration of Anand et al. [65] ($Mg/Ca = 0.38 \times e^{0.09T}$), with variability in estimated calcification temperature that may arise from these different calibrations being <1 °C at Mg/Ca = 0.78 mmol mol^{-1}, the average Mg/Ca composition of MD01-2461 *N. pachyderma* sin. Our calibration overestimates calcification temperatures by 2–3 °C compared to the T–Mg/Ca *N. pachyderma* sin. calibration of Nürnberg et al. [64] ($Mg/Ca = 0.47 \times e^{0.08T}$) using laboratory cultures and Norwegian Sea core top samples. However, early-

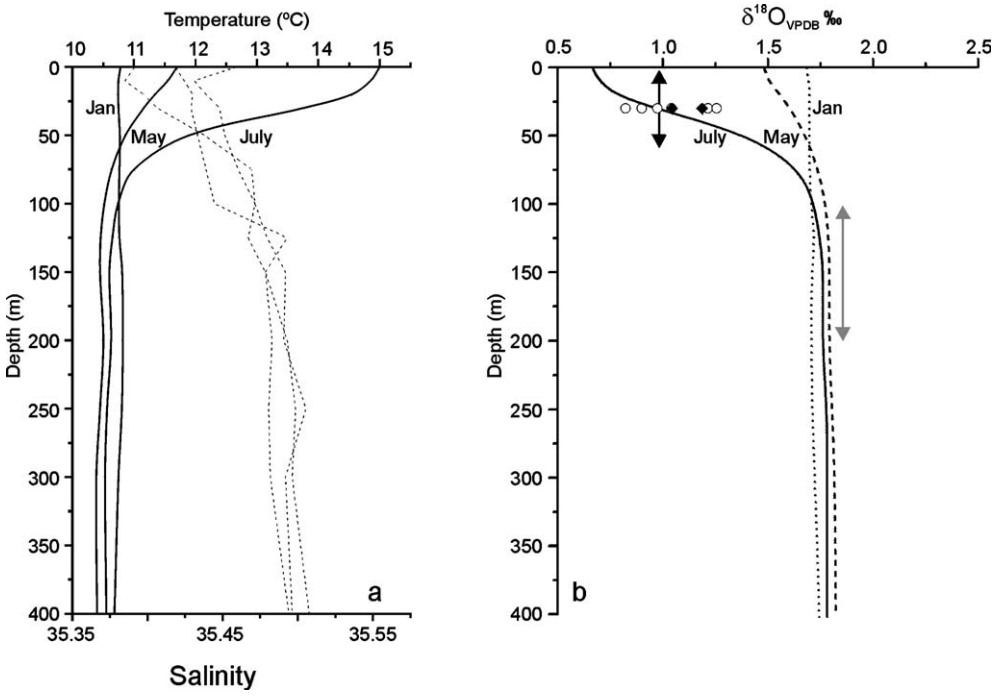

Fig. 5. Modern seawater temperature, salinity, and computed equilibrium $\delta^{18}O_{calcite}$ profiles from MD01-2461. (a) Hydrographic data (temperature - solid lines, salinity - dashed lines) for January, May and July [49]. (b) computed equilibrium $\delta^{18}O_{calcite}$ following [48]. Double-headed arrows locate average calcification depth of *G. bulloides* (black) and *N. pachyderma* sin. (grey). Core top $\delta^{18}O_{G.\ bulloides}$ (open circles from MD01-2461; Black diamonds from box cores 88-06 and 88-07 at 51.4°N and 50.5°N [51]).

Holocene (9.6–8.6 kyr BP) *N. pachyderma* sin. calcification temperatures derived from our calibration average 10.3 °C (unpublished data) and compare well with modern temperatures at a water depth of 150 m (10.6 °C; [49]), substantiating our calibration and suggesting regional differences in the T–Mg/Ca *N. pachyderma* sin. relationship [55]. We consider combined analytical and calibration uncertainties of Mg/Ca-derived temperature estimates to amount to ±1 °C [65].

The resulting temperature record derived from *G. bulloides* Mg/Ca suggests variability of SST within the range 6–16 °C (Fig. 4b), with a SST increase during the early deglacial of ~4 °C. Glacial SST trends derived from *G. bulloides* broadly parallel subsurface temperatures, as determined from *N. pachyderma* sin. Mg/Ca, within the range 6–12 °C (Fig. 4b).

Amplitudes of the temperature anomalies of the two species do not directly mirror the magnitude of coeval excursions in the paired $\delta^{18}O$ records of both species, that on occasion display an anti-phased trend between *G. bulloides* and *N. pachyderma* sin. $\delta^{18}O$ (Fig. 4c). This pattern alludes to changes not only in temperature, but seawater oxygen isotope (δ_w) composition and salinity, with implications for upper ocean water mass stratification. Calcification temperatures, based on Mg/Ca ratios, were used to subtract the temperature component from planktonic $\delta^{18}O$, allowing determination of δ_w following the oxygen isotope palaeotemperature equation of Shackleton [48]. $\delta^{18}O$ values were corrected for global ice volume following [66]. Assuming that the freshwater endmember $\delta^{18}O$ was similar to today, salinity was then determined following the modern North Atlantic δ_w–Salinity relationship, $\delta_w = S \times 0.61 - 21.3$ [67], enabling estimates of density (σ_t) to be made using the International Equation of State of Seawater [68]. Incorporating the errors associated with the analytical precision for Mg/Ca and $\delta^{18}O$, temperature calibration uncertainties and assuming an error of estimate for salinity on δ_w of 0.08 that is derived from the North Atlantic surface δ_w–Salinity relation suggests an uncertainty envelope on density in the range 0.6–0.7 σ_t units. Total error on salinity estimates in the order of ±0.2.

Overlapping density values at the two depth habitats (~30 m for *G. bulloides* and ~150 m for *N. pachyderma* sin.) suggest a well-mixed upper water column at this site for most of the late glacial (Fig. 6b). Elevated $\delta^{13}C_{benthic}$ (>1.5‰; Fig. 6c) during much of this time also suggest rapid ventilation of the mid-depth waters during the late glacial from a nearby source in the open

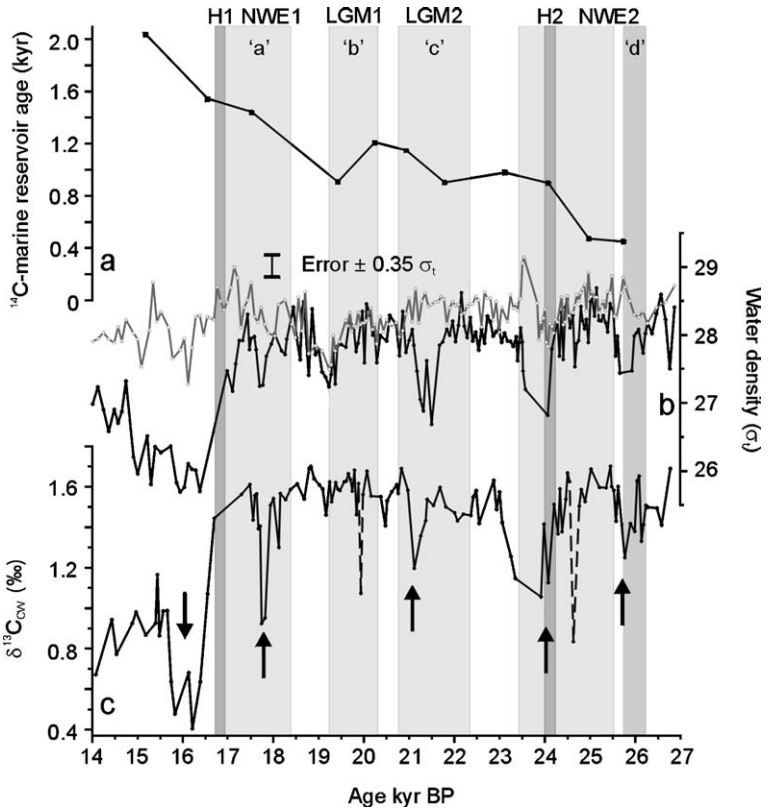

Fig. 6. Upper ocean density profile, intermediate water ventilation and ^{14}C-marine reservoir age proxy records from core MD01-2461. (a) ^{14}C-marine reservoir age (as Fig. 2a). (b) Density (σ_t) for surface (*G. bulloides*; black) and subsurface (*N. pachyderma* sin.; grey) waters. Error bars indicate region of uncertainty in density calculation. (c) δ^{13}C of the benthic foraminifera *Cibicidoides wuellerstorfi*. Vertical bars and abbreviations the same as Fig. 3. Reduced surface density and upper water stratification (b) and associated reductions in δ^{13}C (c) indicated with vertical arrows. Dotted lines in (c) highlight one-point peaks that are potential 'outliers'.

North Atlantic [4,69]. Following H1, SST averages ~4 °C warmer than average LGM temperatures, while a persistent offset of >1‰ is displayed between $\delta^{18}O_{G.\ bulloides}$ and $\delta^{18}O_{N.\ pachyderma\ sin.}$ and a ~0.7‰ reduction in $\delta^{13}C_{benthic}$. This data pattern indicates enhanced surface stratification and concomitant convection slowdown at this site in the course of enhanced meltwater shedding during deglaciation.

Periodic negative excursions in sea surface salinity (SSS) of up to 2.6 suggest recurrent meltwater surges, with fluxes maximising following the major phases of NWEIS instability at NWE2, H2, LGM2 and 1, and NWE1 and finally at H1 (Fig. 4c). The LGM1 salinity reduction peaking at 19.2 kyr BP coincides with the 19-kyr meltwater pulse, supporting the contention [70] that rapid sea level rise of 10–15 m at this time in part originated within the North Atlantic.

These meltwater incursions frequently stratify the upper water column, inferred by divergent surface and subsurface water densities (Fig. 6b). $\delta^{13}C_{benthic}$ depletion by up to 1.2‰ during these episodes suggests reduced intermediate water ventilation, likely reflecting northwards penetration of Antarctic Intermediate Water (AAIW; [4,71]) (Fig. 6c). Several lowered $\delta^{13}C_{benthic}$ data points associated with each NWE meltwater event reinforce the contention that reduced bottom water ventilation at our site, independent of LIS meltwater forcing, is a real feature of these events. Furthermore, each episode of meltwater release, surface stratification and apparent AMOC reduction appears to have had a cumulative effect on the ^{14}C-marine reservoir age at MD01-2461 as each successive event is coincident with a further increase in marine reservoir age (Fig. 6). A temporary reversal in this trend is observed at 19.6 kyr BP, following a period of vigorous AMOC and upper water column mixing at the core site which went some way to 'resetting' the reservoir ages before meltwater associated with NWE1 and H1 caused reservoir ages to increase yet again.

While reduced $\delta^{13}C_{benthic}$ is a well documented feature of H events in the North Atlantic [3–5], reduced bottom water ventilation presented here, associated

exclusively with NWEIS instability and meltwater forcing highlights the significant effect that the smaller circum-North Atlantic ice sheets may have had on AMOC.

3.3. Ice sheet processes in response to ocean–climate forcing

The records of surface and subsurface temperature display fine-scale variability, with salient anomalies that coincide with major IRD events. A notable warm pulse is recorded between 19.0 and 18.6 kyr BP in both surface and subsurface temperatures. A warming pulse at this time, possibly initiating NWEIS instability, has been noted at several core sites west of the British Isles [19,72]. At MD02-2461 this warming occurs over 400 yr and amounts to an increase of ~8 °C for SST and ~5 °C for subsurface temperatures, reaching maxima of 15.6 and 12 °C, respectively at 18.7 kyr BP. An increase in SSS of ~3 associated with this warming pulse may suggest the northward penetration of low latitude, warm saline waters, perhaps reflecting a transient strengthening of the AMOC. Abrupt termination of this warming trend and reduced SSS is associated with initial step-up of NWEIS debris flux at 18.4 kyr BP, NWE1.

Increased upper ocean temperatures prior to IRD deposition derived from the NWEIS suggests an intensification of ocean thermal forcing may have led to basal melt of ice shelves fringing these ice sheets and retreat of the grounding line [73,74]. At the same time heat exchange with the atmosphere may have increased surface melt, accelerating ice shelf break up [75] and ice stream flow [76]. Increased ice accumulation on the BIS, caused by increased precipitation from a warmed atmosphere, possibly increased the interior ice sheet mass and thereby reduced stability further [77]. Close coupling of ocean–climate and BIS stability is envisaged. It is suggested that BIS instability initiating NWE2, recorded by moderate BIS-IRD deposition, may have resulted from ice shelf break-up due to surface–subsurface warming above a critical threshold (cf. [73,75,78]). Within the 300 yr duration of this phase, sufficient ice shelf was melted back to reduce any buttressing effect, triggering fast flow of tributary ice streams [79] producing the large and abrupt increase in IRD deposition during the peak of the NWE2 event at 25.0 kyr BP. Accelerated ice stream activity appears to have lasted for ~300 yr, during which IRD deposition remained high and sufficient freshwater was released to stabilise the upper water column and reduce intermediate water ventilation. After this unstable phase, the NWEIS, principally the BIS, appear to have restabilised, reducing IRD delivery and perhaps allowing ice volume to recover. Were collapse of the LIS interpreted to be in response to the same forcing as the NWEIS (cf. [18]) a response time of almost 2 kyr in excess of the NWEIS may be implied from our records. As such, it may be perceived that the so-called European 'precursor' events were not directly linked to the H events (cf. [17]), but were rather a manifestation of differing ice sheet response times to a common forcing, conceivably reflecting the greater mass of the LIS supporting a high thermal inertia and/or time taken for ocean warming to reach ice shelves buttressing the LIS. Limited marine-based BIS margins, and therefore greater ice sheet stability by the time of H1, following the retreat of the Irish Sea ice stream [80], may account for the high rise in surface and subsurface temperatures apparently required to initiate BIS instability at NWE1 compared to NWE2.

The major influx of local BIS debris immediately following deposition of H layer 2 includes the shallow benthic foraminifera *Elphidium excavatum forma clavata* which suggests down-slope transportation from a proximal glaciomarine source [81]. Assuming marine margins remained, it seems plausible that increased SSTs, exceeding 10 °C, would have destabilised the BIS margin further, enhancing calving and initiating debris flow down the continental slope. A rise in sea level of 10 to 15 m associated with the collapse of the LIS [82,83] may also have contributed to this destabilisation [18]. The near absence of locally derived IRD coincident with or following H1 suggests that the BIS ice margin had retreated sufficiently to be unaffected by a SST or sea level change associated with LIS collapse, or that exposed sea floor within the Irish Sea limited iceberg entry into the open ocean, glacial runoff freshening surface waters as opposed to ice rafting.

3.4. NW European ice sheet instability and AMOC variability

Decreased mid-depth water ventilation prior to the main LIS collapse events at H1 and H2 are noted in $\delta^{13}C_{benthic}$ records throughout the North Atlantic [3–5,71]. Whereas the decline of intermediate water ventilation is often progressive in these records, beginning up to 2.5 kyr before full H conditions (H1; [4]), $\delta^{13}C_{benthic}$ at our site records temporary, 200–400 yr, reduction in intermediate-water ventilation, associated with NWEIS instability/meltwater forcing, 1.2–1.8 kyr before full H event conditions. $\delta^{13}C_{benthic}$ at MD01-2461 then decreases again associated with and following LIS-sourced IRD deposition and further meltwater

release, in phase with records of complete AMOC collapse [71]. Given that advance of AAIW to MD01-2461 was likely in compensation for reduced Glacial North Atlantic Intermediate Water (GNAIW) formation [71], far-reaching effects of the NWEIS-sourced meltwater pulses may be implied prior to both H1 and H2. It is envisaged that NWEIS-sourced meltwater extended to the area of GNAIW formation, weakening deep/intermediate water production and reducing AMOC. Had the meltwater pulses produced longer-term stratification of surface waters within this region than is observed at MD01-2461 they may account for the progressive, pre-H event spin-down of AMOC recorded at more southerly sites [4].

4. Summary

We demonstrate the apparent sensitivity and heightened response of the NWEIS to climatic warming with respect to the well grounded, stable LIS during the last glacial period. Despite the comparatively small ice volume of the NWEIS, their positioning with respect to the likely centre of last glacial North Atlantic deep or intermediate water formation appears to have made meltwater released from the NWEIS an effective means of causing basin wide AMOC variability, highlighting the important role of the NWEIS in millennial scale climatic events.

Acknowledgements

We thank H.J. Medley and B.T. Long for sample preparation, R.T. Chaudri for assistance with AMS sample preparation, M.J. Greaves for sharing his expertise in Mg/Ca analysis and G.G. Bianchi for stable isotope analysis. We are grateful to J.T. Andrews and H. Rashid for their constructive comments that greatly improved this manuscript. This work was funded by the Natural Environment Research Council.

References

[1] A. Ganopolski, S. Rahmstorf, Rapid changes of glacial climate simulated in a coupled climate model, Nature 409 (2001) 153–158.

[2] S. Charbit, C. Ritz, G. Ramstein, Simulations of Northern Hemisphere ice-sheet retreat: sensitivity to physical mechanisms involved during the last deglaciation, Quat. Sci. Rev. 21 (2002) 243–265.

[3] L. Vidal, L. Labeyrie, E. Cortijo, M. Arnold, J.C. Duplessy, E. Michel, S. Becqué, T.C.E. van Weering, Evidence for changes in the North Atlantic deep water linked to meltwater surges during the Heinrich events, Earth Planet. Sci. Lett. 146 (1997) 13–27.

[4] R. Zahn, J. Schonfeld, H.R. Kudrass, M.H. Park, H. Erlenkeuser, P. Grootes, Thermohaline instability in the North Atlantic during meltwater events: stable isotope and ice-rafted detritus records from core SO75-26KL, Portuguese margin, Paleoceanography 12 (1997) 696–710.

[5] M. Elliot, L. Labeyrie, J.C. Duplessy, Changes in North Atlantic deep-water formation associated with the Dansgaard–Oeschger temperature oscillations (60–10 kyr), Quat. Sci. Rev. 21 (2002) 1153–1165.

[6] S.R. Hemming, Heinrich events: massive Late Pleistocene detritus layers of the North Atlantic and their global climate imprint, Rev. Geophys. 42 (2004) RG 1005, doi:10.1029/2003RG000128.

[7] G.C. Bond, R. Lotti, Iceberg discharges into the North Atlantic on millennial time scales during the last glaciation, Science 267 (1995) 1005–1010.

[8] K.S. Lackschewitz, K.H. Baumann, B. Gehrke, H.J. Wallrabe-Adams, J. Thiede, G. Bonani, R. Endler, H. Erlenkeuser, J. Heinemeier, North Atlantic ice sheet fluctuations 10,000–70,000 yr ago as inferred from deposits on the Reykjanes ridge, southeast of Greenland, Quat. Res. 49 (1998) 171–182.

[9] G. Bond, W. Showers, M. Cheseby, R. Lotti, P. Almasi, P. deMenocal, P. Priore, H. Cullen, I. Hajdas, G. Bonani, A pervasive millennial-scale cycle in North Atlantic Holocene and glacial climates, Science 278 (1997) 1257–1266.

[10] D.R. MacAyeal, Binge/purge oscillations of the Laurentide ice sheet as a cause of the North Atlantic′s Heinrich events, Paleoceanography 8 (1993) 775–784.

[11] S.J. Marshall, G.K.C. Clarke, A continuum mixture model of ice stream thermomechanics in the Laurentide Ice Sheet: 2. Application to the Hudson Strait Ice Stream, J. Geophys. Res., [Solid Earth] 102 (1997) 20615–20637.

[12] J.T. Andrews, D.C. Barber, Dansgaard–Oeschger events: is there a signal off the Hudson Strait ice stream? Quat. Sci. Rev. 21 (2002) 443–454.

[13] R.B. Alley, D.R. MacAyeal, Ice-rafted debris associated with binge–purge oscillations of the Laurentide Ice Sheet, Paleoceanography 9 (1994) 503–511.

[14] T. Fronval, E. Jansen, J. Bloemendal, S. Johnsen, Oceanic evidence for coherent fluctuations in Fennoscandian and Laurentide ice sheets on millennium timescales, Nature 374 (1995) 443–446.

[15] M. Elliot, L. Labeyrie, G. Bond, E. Cortijo, J.L. Turon, N. Tisnerat, J.C. Duplessy, Millennial-scale iceberg discharges in the Irminger Basin during the last glacial period, relationship with the Heinrich events and environmental settings, Paleoceanography 13 (1998) 433–446.

[16] P.C. Knutz, W.E.N. Austin, E.J.W. Jones, Millennial scale depositional cycles related to British Ice Sheet variability and North Atlantic palaeocirculation since 45 ka B.P. Barra Fan, U.K. margin, Paleoceanography 16 (2001) 53–64.

[17] F.E. Grousset, C. Pujol, L. Labeyrie, G. Auffret, A. Boelaert, Were the North Atlantic Heinrich events triggered by the behavior of the European ice sheets? Geology 28 (2000) 123–126.

[18] J.D. Scourse, I.R. Hall, I.N. McCave, J.R. Young, C. Sugdon, The origin of Heinrich layers: evidence from H2 for European precursor events, Earth Planet. Sci. Lett. 182 (2000) 187–195.

[19] P.C. Knutz, I.R. Hall, R. Zahn, T.L. Rassmussen, A. Kuijpers, M. Moros, N.J. Shackleton, Multidecadal ocean variability and NW European ice sheet surges during the last deglaciation, Geochem. Geophys. Geosyst. 3 (2002) 1077.

[20] G. Bond, H. Heinrich, W. Broecker, L. Labeyrie, J. McManus, J. Andrews, S. Huon, R. Jantschik, S. Clasen, C. Simet, K. Tedesco, M. Klas, G. Bonani, S. Ivy, Evidence for massive discharges of icebergs into the North Atlantic Ocean during the last glacial period, Nature 360 (1992) 245–249.

[21] G. Bond, W. Broecker, S. Johnsen, J. McManus, L. Labeyrie, J. Jouzel, G. Bonani, Correlations between climate records from North Atlantic sediments and Greenland ice, Nature 365 (1993) 143–147.

[22] J.D. Scourse, M.F.A. Furze, A critical review of the glaciomarine model for Irish sea deglaciation: evidence from southern Britain, the Celtic shelf and adjacent continental slope, J. Quat. Sci. 16 (2001) 419–434.

[23] F.E. Grousset, L. Labeyrie, J.A. Sinko, M. Cremer, G. Bond, J. Duprat, E. Cortijo, S. Huon, Patterns of ice-rafted detritus in the glacial North Atlantic (40–55°N), Paleoceanography 8 (1993) 175–192.

[24] S. Zaragosi, F. Eynaud, C. Pujol, G.A. Auffret, J.L. Turon, T. Garland, Initiation of the European deglaciation as recorded in the northwestern Bay of Biscay slope environments (Meriadzek Terrace and Trevelyan Escarpment), a multi-proxy approach, Earth Planet. Sci. Lett. 188 (2001) 493–507.

[25] W.F. Ruddiman, Late Quaternary deposition of ice-rafted sand in the sub-polar North Atlantic (lat 40° to 65°), Geol. Soc. Amer. Bull. 88 (1977) 1813–1821.

[26] M. Stuiver, P.J. Reimer, R.W. Reimer, CALIB 5.0, http://calib.qub.ac.uk/calib/2005.

[27] A.W.H. Bé, An ecological, zoogeographic and taxonomic review of recent planktonic foraminifera, Oceanic Micropaleontology, Academic Press, New York, 1977, pp. 1–100.

[28] P.M. Grootes, M. Stuiver, Oxygen 18/16 variability in Greenland snow and ice with 10(−3)- to 10(5)-year time resolution, J. Geophys. Res.,Oceans 102 (1997) 26455–26470 (http://depts.washington.edu/qil/datasets/gisp2_main.html).

[29] W.E.N. Austin, E. Bard, J.B. Hunt, D. Kroon, J.D. Peacock, The C-14 age of the Icelandic Vedde Ash — implications for younger Dryas marine reservoir age corrections, Radiocarbon 37 (1997) 53–62.

[30] A.H.L. Voelker, M. Sarnthein, P.M. Grootes, H. Erlenkeuser, C. Laj, A. Mazaud, M.J. Nadeau, M. Schleicher, Correlation of marine C-14 ages from the Nordic Seas with the GISP2 isotope record: implications for C-14 calibration beyond 25 ka BP, Radiocarbon 40 (1998) 517–534.

[31] C. Waelbroeck, J.C. Duplessy, E. Michel, L. Labeyrie, D. Paillard, J. Duprat, The timing of the last deglaciation in North Atlantic climate records, Nature 412 (2001) 724–727.

[32] J. Eiriksson, G. Larsen, K.L. Knudsen, J. Heinemeier, L.A. Simonarson, Marine reservoir age variability and water mass distribution in the Iceland Sea, Quat. Sci. Rev. 23 (2004) 2247–2268.

[33] E.W. Domack, A.J.T. Jull, J.B. Anderson, T.W. Linick, C.R. Williams, Application of tandem accelerator mass-spectrometer dating to late Pleistocene–Holocene sediments of the East Antarctic continental shelf, Quat. Res. 31 (1989) 277–287.

[34] C.C. Veiga-Pires, C. Hillaire-Marcel, U and Th isotope constraints on the duration of Heinrich events H0–H4 in the southeastern Labrador Sea, Paleoceanography 14 (1999) 187–199.

[35] J.T. Andrews, K. Tedesco, Detrital carbonate-rich sediments, north-western Labrador Sea: implications for ice-sheet dynamics and iceberg rafting (Heinrich) events in the North Atlantic, Geology 20 (1992) 1087–1090.

[36] F.E. Grousset, M. Parra, A. Bory, P. Martinez, P. Bertrand, G. Shimmield, R. Ellam, Saharan wind regimes traced by the Sr–Nd isotopic composition of the tropical Atlantic sediments: last glacial maximum vs today, Quat. Sci. Rev. 17 (1998) 395–409.

[37] S.D. Samon, E.C. Alexander Jr., Calibration of the interlaboratory ^{40}Ar–^{39}Ar dating standard, MMhb-1, Chem. Geol. (Isotope Geoscience Section) 66 (1987) 27–34.

[38] S.R. Hemming, W.S. Broecker, W.D. Sharp, G.C. Bond, R.H. Gwiazda, J.F. McManus, M. Klas, I. Hajdas, Provenance of Heinrich layers in core V28–82, northeastern Atlantic: $^{40}Ar/^{39}Ar$ ages of ice-rafted hornblende, Pb isotopes in feldspar grains, and Nd–Sr–Pb isotopes in the fine sediment fraction, Earth Planet. Sci. Lett. 164 (1998) 317–333.

[39] S.R. Hemming, G.C. Bond, W.S. Broecker, W.D. Sharp, M. Klas-Mendelson, Evidence from $^{40}Ar/^{39}Ar$ ages of individual hornblende grains for varying Laurentide sources of iceberg discharges 22,000 to 10,500 14C yr B.P. Quat. Res. 54 (2000) 372–383.

[40] S.R. Hemming, I. Hajdas, Ice-rafted detritus evidence from Ar-40/Ar-39 ages of individual hornblende grains for evolution of the eastern margin of the Laurentide ice sheet since 43 C-14 ky, Quat. Int. 99 (2000) 29–43.

[41] V.L. Peck, I.R. Hall, R. Zahn, F.E. Grousset, J.D. Scourse, The relationship of Heinrich events and their European precursors over the past 60 kyr BP: a multi-proxy ice rafted debris provenance study in the North East Atlantic Quat. Sci. Rev., submitted for publication.

[42] S. Barker, M. Greaves, H. Elderfield, A study of cleaning procedures used for foraminiferal Mg/Ca paleothermometry, Geochem. Geophys. Geosyst. 4 (2003) 8407, doi:10.1029/2003GC000559.

[43] E.R. Wadsworth, PhD Thesis, The identification and characterisation of the North Atlantic Heinrich events using environmental magnetic techniques, St. Andrews (2005).

[44] H. Snoeckx, F. Grousset, M. Revel, A. Boelaert, European contribution of ice-rafted sand to Heinrich layers H3 and H4, Mar. Geol. 158 (1999) 197–208.

[45] F.E. Grousset, E. Cortijo, S. Huon, L. Herve, T. Richter, D. Burdloff, J. Duprat, O. Weber, Zooming in on Heinrich layers, Paleoceanography 16 (2001) 240–259.

[46] C. Hillare-Marcel, G. Bilodeau, Instabilities in the Labrador Sea mass structure during the last climate cycle, Can. J. Earth Sci. 37 (2000) 795–809.

[47] J. Simstich, M. Sarnthein, H. Erlenkeuser, Paired delta O-18 signals of *Neogloboquadrina pachyderma* (s) and *Turborotalita quinqueloba* show thermal stratification structure in Nordic Seas, Mar. Micropaleontol. 48 (2003) 107–125.

[48] N.J. Shackleton, Attainment of isotopic equilibrium between ocean water and the benthonic foraminifer genus *Uvigerina*: isotopic changes in the ocean during the last glacial, vol. 219, Collogue CNRS Centre National de la Recherche Scientifique, Paris, 1974, pp. 203–210.

[49] NODC (Levitus) World Ocean Atlas, 1998, data provided by the NOAA-CIRES Climate Diagnostics Center, Boulder, Colorado, USA, from their Web site at http://www.cdc.noaa.gov/.

[50] S. Barker, H. Elderfield, Foraminiferal calcification response to glacial–interglacial changes in atmospheric CO_2, Science 297 (2002) 833–836.

[51] G.M. Ganssen, D. Kroon, The isotopic signature of planktonic foraminifera from the NE Atlantic surface sediments:

implications for the reconstruction of past oceanic conditions, J. Geol. Soc. (Lond.) 157 (2000) 693–699.
[52] J. Carstens, D. Hebbeln, G. Wefer, Distribution of planktic foraminifera at the ice margin in the Arctic (Fram Strait), Mar. Micropaleontol. 29 (1997) 257–269.
[53] K.E. Kohfeld, R.G. Fairbanks, S.L. Smith, I.D. Walsh, *Neogloboquadrina pachyderma* (sinistral coiling) as paleoceanographic tracers in polar waters: evidence from Northeast Water Polyna plankton tows, sediment traps, and surface sediments, Paleoceanography 11 (1996) 679–699.
[54] R. Volkmann, Planktic foraminifers in the outer Laptev Sea and the Fram Strait—modern distribution and ecology, J. Foraminiferal Res. 30 (2000) 157–176.
[55] D.N. Nürnberg, Magnesium in tests of *Neogloboquadrina pachyderma* sinistral from high northern and southern latitudes, J. Foraminiferal Res. 25 (1995) 350–368.
[56] J.T. Durazzi, Stable isotope studies of planktonic-foraminifera in North Atlantic core tops, Palaeogeogr. Palaeoclimatol. Palaeoecol. 33 (1981) 157–172.
[57] R.F. Spielhagen, H. Erlenkeuser, Stable oxygen and carbon isotopes in planktonic foraminifera from Arctic Ocean surface sediments — reflection of the low-salinity surface water layer, Geology 119 (1994) 227–250.
[58] G.P. Wu, C. Hillaire Marcel, Oxygen isotope compositions of sinistral *Neogloboquadrina-pachyderma* tests in surface sediments — North Atlantic Ocean, Geochim. Cosmochim. Acta 58 (1994) 1303–1312.
[59] D. Bauch, J. Carstens, G. Wefer, Oxygen isotope composition of living *Neogloboquadrina pachyderma* (sin) in the Arctic Ocean, Earth Planet. Sci. Lett. 146 (1997) 47–58.
[60] R. Volkmann, M. Mensch, Stable isotope composition (delta O-18, delta C-13) of living planktic foraminifers in the outer Laptev Sea and the Fram Strait, Mar. Micropaleontol. 42 (2001) 163–188.
[61] H. Elderfield, G. Ganssen, Past temperature and $\delta^{18}O$ of surface ocean waters inferred from foraminiferal Mg/Ca ratios, Nature 405 (2000) 442–445.
[62] T.A. Mashiotta, D.W. Lea, H.J. Spero, Glacial–interglacial changes in Subantarctic sea surface temperature and delta O-18-water using foraminiferal Mg, Earth Planet. Sci. Lett. 170 (1999) 417–432.
[63] M.A. Maslin, N.J. Shackleton, U. Pflaumann, Surface water temperature, salinity and density changes in the northeast Atlantic during the last 45,000 years: Heinrich events, deep water formation, and climatic rebounds, Paleoceanography 10 (1995) 527–544.
[64] D. Nürnberg, J. Bijma, C. Hemleben, Assessing the reliability of magnesium in foraminiferal calcite as a proxy for water mass temperatures, Geochim. Cosmochim. Acta 60 (1996) 803–814.
[65] P.H. Anand, H. Elderfield, H. Conte, Calibration of Mg/Ca thermometry in planktonic foraminifers from a sediment trap time series, Palaeoceanography 18 (2003) 1050, doi:10.1029/2002PA000846.
[66] N.J. Shackleton, The 100,000-year ice age cycle identified and found to lag temperature, carbon dioxide and orbital eccentricity, Science 289 (2000) 1897–1902.
[67] H. Craig, L.I. Gordon, Deuterium and oxygen 18 variations in the ocean and the marine atmosphere, in: E. Tongiorgi (Ed.), Stable Isotopes in Oceano-graphic Studies and Paleotemperatures, Lab. di Geol. Nucl.,Cons. Naz. delle Ric., Pisa, Italy, 1965, pp. 9–130.
[68] UNESCO background papers and supporting data on the International Equation of State of Seawater 1980, UNESCO Technical Papers in Marine Science, vol. 38, 1980, p. 192.
[69] D.W. Oppo, S.J. Lehman, Mid-depth circulation of the subpolar North Atlantic during the last glacial maximum, Science 259 (1993) 1148–1152.
[70] P.U. Clark, A.M. McCabe, A.C. Mix, A.J. Weaver, Rapid rise of sea level 19,000 years ago and its global implications, Science 304 (2004) 1141–1144.
[71] R. Rickaby, H. Elderfield, Evidence from the high-latitude North Atlantic for variations in Antarctic intermediate water flow during the last deglaciation, Geochem. Geophys. Geosyst. 6 (2005), doi:10.1029/2004GC000858.
[72] I.M. Lagerklint, J.D. Wright, Late glacial warming prior to Heinrich event: 1. The influence of ice rafting and large ice sheets on the timing of initial warming, Geology 27 (1999) 1099–1102.
[73] E. Rignot, S.S. Jacobs, Rapid bottom melting widespread near Antarctic ice sheet grounding lines, Science 296 (2002) 2020–2023.
[74] G. Shaffer, S.M. Olsen, C.J. Bjerrum, Ocean subsurface warming as a mechanism for coupling Dansgaard–Oeschger climate cycles and ice-rafting events, Geophys. Res. Lett. 31 (2004) L24202, doi:10.1029/2004GL020968.
[75] D.R. MacAyeal, T.A. Scambos, C.L. Hulbe, M.A. Fahnestock, Catastrophic ice-shelf break-up by an ice-shelf-fragment-capsize mechanism, J. Glaciol. 49 (2003) 2–36.
[76] H.J. Zwally, W. Abdalati, T. Herring, K. Larson, J. Saba, K. Steffen, Surface melt-induced acceleration of Greenland ice-sheet flow, Science 297 (2002) 218–222.
[77] M. Oppenheimer, Global warming and the stability of the West Antarctic ice sheet, Nature 393 (1998) 325–332.
[78] D.G. Vaughan, C.S.M. Doake, Recent atmospheric warming and retreat of ice shelves on the Antarctic Peninsula, Nature 379 (1996) 328–331.
[79] H. De Angelis, P. Skvarca, Glacier surge after ice shelf collapse, Science 299 (2003) 1560–1562.
[80] A.M. McCabe, P.U. Clark, Ice-sheet variability around the North Atlantic Ocean during the last deglaciation, Nature 392 (1998) 373–377.
[81] L.E. Osterman, Benthic foraminiferal zonation of a glacial–interglacial transition from Frobisher Bay, Baffin Island, N.W.T., Canada, in: H.J. Oertli (Ed.), Benthos ′83, 1984, pp. 471–476.
[82] J. Chappell, Sea level changes forced ice breakouts in the last glacial cycle: new results from coral terraces, Quat. Sci. Rev. 21 (2002) 1229–1240.
[83] Y. Yokoyama, T.M. Esat, K. Lambeck, Coupled climate and sea-level changes deduced from Huon Peninsula coral terraces of the last ice age, Earth Planet. Sci. Lett. 193 (2001) 579–587.